



1                   **Stratospheric observations of noctilucent clouds: a new approach in**  
2                   **studying large-scale mesospheric dynamics**

3           Peter Dalin<sup>1,2,\*</sup>, Nikolay Pertsev<sup>3</sup>, Vladimir Perminov<sup>3</sup>, Denis Efremov<sup>4,5</sup>, Vitaly Romejko<sup>6</sup>

4  
5           <sup>1</sup> Swedish Institute of Space Physics, Box 812, SE-981 28 Kiruna, Sweden

6           <sup>2</sup> Space Research Institute, RAS, Profsovnaya st. 84/32, Moscow, 117997, Russia

7           <sup>3</sup> A.M. Obukhov Institute of Atmospheric Physics, RAS, Pyzhevskiy per. 3, Moscow, 119017, Russia

8           <sup>4</sup> Aerospace laboratory ðStratonauticaö, Moscow, Russia

9           <sup>5</sup> Faculty of Cosmic Research, M.V. Lomonosov Moscow State University, GSP-1, Leninskie  
10           Gory, Moscow, 119991, Russia

11           <sup>6</sup> The Moscow Association for NLC Research, Kosygina st. 17, Moscow, 119334, Russia

12

13           \*Corresponding author at: Swedish Institute of Space Physics, Box 812, SE-981 28 Kiruna,  
14           Sweden. Fax: +46 980 79050. E-mail address: pdalin@irf.se (P. Dalin).

15

16           **Abstract.**

17           The experimental campaign Stratospheric Observations of Noctilucent Clouds (SONC)  
18           was conducted on the night of 5-6 July 2018 with the aim of photographing noctilucent clouds  
19           (NLC) and studying their large-scale spatial dynamics at scales of 1000–1450 km. An  
20           automated high-resolution camera (equipped with a wide-angle lens) was lifted by a  
21           stratospheric sounding balloon to 20.4 km altitude above the Moscow region in Russia  
22           (~56°N; 41°E), taking several hundreds of NLC images during the flight that lasted 1.7  
23           hours. The combination of a high-resolution camera and large geographic coverage (~1500  
24           km) have provided a unique technique of NLC observations from the stratosphere, which is  
25           impossible to currently achieve either from the ground or space. We have estimated that a  
26           horizontal extension of the NLC field as seen from the balloon was about 1450 x 750 km  
27           whereas it was about 800 x 550 km as seen from the ground. The NLC field was located in a  
28           cold area of the mesopause (136-146 K), which is confirmed by satellite measurements. The  
29           southmost edge of the NLC field was modulated by partial ice voids of 150-250 km in  
30           diameter. A medium-scale gravity wave had a wavelength of 49.4±2.2 km with vertical  
31           amplitude of 1.9±0.1 km. The final state of the NLC evolution was represented by thin  
32           parallel gravity wave stripes. Balloon-borne observations provide new horizons in studies of  
33           NLC at various distances from metres to thousands of km.



34

35 *Keywords:* noctilucent clouds, mesospheric dynamics, balloon-borne stratospheric  
36 observations, atmospheric gravity waves

37

## 38 **1 Introduction**

39 Night-shining clouds or noctilucent clouds (NLC) are the highest clouds in the Earth's  
40 atmosphere observed at the summer mesopause between 80 and 90 km. NLC can be readily  
41 seen from mid- and subpolar latitudes of both hemispheres. NLC are composed of water-ice  
42 particles of 300–100 nm in radius that scatter sunlight and thus NLCs are observed against the  
43 dark twilight arc from May until September in the Northern Hemisphere and from November  
44 to February in the Southern Hemisphere (Bronshten and Grishin, 1970; Gadsden and  
45 Schröder, 1989; Liu et al., 2016). NLC are also observed from space and in this case they are  
46 usually called Polar Mesospheric Clouds (PMC) (Thomas, 1984).

47 NLC are almost always represented by a wave surface having a complex interplay  
48 between small-scale turbulence processes of 10–1000 metres, atmospheric gravity waves  
49 (GW) with wavelengths of 10–1000 km, planetary waves, solar thermal tides and lunar  
50 gravitational tides of about 10000 km (Witt, 1962; Fritts et al., 1993; Rapp et al., 2002;  
51 Kirkwood and Stebel, 2003; Chandran et al., 2009; Dalin et al., 2010; Fiedler et al., 2011;  
52 Taylor et al., 2011; Pertsev et al., 2015). Sometimes, distinguished non-linear mesospheric  
53 phenomena like mesospheric walls or fronts appear at the mesopause which clearly separate  
54 two volumes of the mesopause having cold and warm air masses with temperature difference  
55 of 20–25 K across a few km (Dubietis et al., 2011; Dalin et al., 2013).

56 NLC/PMC are systematically observed and studied from the ground (optical imagers,  
57 lidars), as well as from space (AIM, Odin, SBUV instruments) (e.g., Karlsson and Gumbel,  
58 2005; Dalin et al., 2008; Bailey et al., 2009; Fiedler et al., 2011; DeLand and Thomas, 2015);  
59 there are also irregular (campaign-based) NLC observations conducted by using sounding  
60 rockets and aircraft (Zadorozhny et al., 1993; Gumbel and Witt, 2001; Reimuller et al., 2011).  
61 These techniques have advantages and disadvantages. In particular, ground-based  
62 measurements provide a high horizontal resolution of ~20 m and high temporal resolution of  
63 seconds (optical imagers) (Dalin et al., 2010; Baumgarten and Fritts, 2014) and high vertical  
64 resolution of 50–150 metres using lidars (Baumgarten et al., 2009) but are limited to  
65 tropospheric weather conditions and restricted to a certain small region on the Earth's surface.



66 Satellite measurements, on the other hand, provide global PMC coverage but have low spatial  
67 horizontal resolution (~5 km) as well as large spatial gaps of several hundreds of km between  
68 adjacent orbits at middle and subpolar latitudes. Thus, there is no perfect technique to observe  
69 and study NLC/PMC so far. There is an obvious methodological gap in these techniques,  
70 resulting in a gap of stratospheric altitudes (20-40 km), which are potentially available for  
71 comprehensive studies of NLC/PMC. This gap is due to lack of systematic stratospheric  
72 balloon-borne experiments aiming at NLC/PMC observations. So far, there has been  
73 conducted a single published experiment from a stratospheric balloon providing PMC  
74 observations over Antarctica between 29 December 2012 and 9 January 2013 (Miller et al.,  
75 2015). The E and B Experiment (EBEX) was dedicated to another research field concerning  
76 polarization in the cosmic microwave background (Reichborn-Kjennerud et al., 2010). At the  
77 same time, two star cameras of the EBEX experiment, having a narrow field of view of  $4.1^\circ \times$   
78  $2.7^\circ$ , were able to register fine structures of PMC and turbulence dynamics, ranging from  
79 several km down to 10 m. Another balloon-borne experiment (PMC-Turbo) was conducted  
80 between 8 and 14 July 2018 over Sweden-Greenland-Canada territories in order to capture  
81 NLC with seven optical cameras and lidar (Fritts et al., 2019). The PMC-Turbo experiment  
82 was launched about 2.5 days after the experiment described in the present paper.

83 In this paper, we report on scientific results of a new balloon-borne experiment dedicated  
84 to studies of NLC large-scale dynamics at horizontal scales of more than 100 km (Dalin et al.,  
85 2019). Such experiment, conducted for the first time, opens new horizons for studies of large-  
86 scale dynamical features in combination with a high spatial resolution at the summer  
87 mesopause, currently unachievable for other techniques like ground-based and space  
88 measurements.

89

## 90 **2 Technique and method**

91 The Stratospheric Observations of Noctilucent Clouds (SONC) experiment is a special  
92 balloon-borne experiment dedicated to studies of large-scale dynamical features in NLC. A  
93 high resolution high sensitive camera (Sony Alpha A7S), having a full frame 35 mm 12  
94 megapixel sensor (4240 x 2832 pixels) and equipped with a wide-angle lens (field of view,  
95 FoV, is  $109.7^\circ \times 81.6^\circ$ ), has been installed on a meteorological sounding balloon. This  
96 combination of a high resolution sensor and wide FoV yields spatial horizontal resolutions of  
97 ~30 m and ~3000 m, when looking at 83 km from 20 km at elevation angles of  $90^\circ$  and  $0^\circ$ ,  
98 respectively. The horizontal coverage of a mesopause layer is over 2000 km, when viewing  
99 along the horizon at low elevation angles. The balloon was launched from the Moscow



100 region, Russia ( $\sim 56^{\circ}\text{N}$ ;  $41^{\circ}\text{E}$ ), on the night of 5-6 July 2018. Since a gondola payload is  
101 constantly rotating and shaking during its flight, the NLC camera was installed on a special  
102 stabilized platform. The 3-axis motorized gimbal stabilized platform (Fig. 1) was designed  
103 and build by the Aerospace laboratory "Stratonautica" (<http://stratonautica.ru>), which has a  
104 wide experience in building such platforms and launching sounding balloons. The platform  
105 was designed to rotate in a  $60^{\circ}$  step in the azimuth angle in order to capture the whole  
106 hemisphere ( $360^{\circ}$ ) since NLC can appear in any direction as observed from mid-latitudes,  
107 including the southern part of the sky (Hultgren et al., 2011; Suzuki et al., 2016). The NLC  
108 camera took images every 6 s during the whole flight, obtained several thousands of images  
109 and several hundreds of images capturing NLC. Besides, automatic exposure bracketing was  
110 used to take four images in sequence with different exposures, allowing us to register various  
111 NLC brightness from very bright to very faint as well as faint stars, which are important  
112 information for the photogrammetric technique and georeference procedure of the images.

113 The balloon was launched at 21:34 UT on 5 July 2018 and the total flight duration was  
114 about 1.7 hours. The ascent speed was around 5 m/s and the balloon reached its maximum  
115 altitude of 20.4 km where it burst; then the payload descended with a parachute and the  
116 payload was successfully recovered. A GPS receiver was installed onboard in order to obtain  
117 information on the balloon trajectory. The flight characteristics of the SONC balloon are  
118 shown in Fig. 2.

119 A ground-based support consisting of three automated NLC cameras was established in  
120 the Moscow region in order to launch the balloon at the time of NLC appearance. Also, a  
121 number of amateur observers significantly contributed to the NLC observational programme  
122 before and during the flight. A launch window was preliminary chosen at the beginning of  
123 July based on long-term statistics of NLC observations conducted in the Moscow region since  
124 1962 to present time. This statistics demonstrate that NLC appear at the beginning of July  
125 with about 65% occurrence probability on a clear night.

126

### 127 **3 The observation**

128 During the flight, the balloon-borne camera captured an extended NLC field with a  
129 number of interesting features discussed in section 4. One can note the following general  
130 characteristics of the NLC display:

131 a) NLC were observed between 20:30 and 23:15 UT on 5 July 2018.



132        b) NLC were located between 82.6 and 85.1 km. The NLC height was estimated by using  
133        synchronously taken images obtained from two ground-based cameras located in the Moscow  
134        region.

135        c) NLC field extended along the horizon from NW to NE at low elevation angles from  $65^\circ$   
136        to  $+11^\circ$  as seen from the balloon.

137        d) NLC were modulated by atmospheric gravity waves of various scales having horizontal  
138        wavelength from 9 km to 50 km.

139        e) NLC were traveling in a rather unusual direction from the south to north at the observed  
140        mean speed of  $\sim 43$  m/s.

141        f) NLC were fading during the balloon ascent and they got very faint and less structured at  
142        the maximum balloon altitude of 20.4 km. The brightest and well-developed NLC were  
143        observed when the SONC balloon was between 6 and 13 km, that is why we analyze the most  
144        profound features of NLC images obtained at this height range.

145        Each analyzed NLC image was georeferenced using horizontal coordinates of referenced  
146        stars (at least 15 stars are needed). The technique of the NLC georeference, triangulation  
147        height estimation and error analysis can be found in Dalin et al. (2004, 2015).

148

#### 149        **4 Results and discussion**

150        The projection of the NLC field on the surface along with the temperature map obtained  
151        with the Aura/MLS spectrometer is shown in Fig. 3. The description on the MLS temperature  
152        product and its validation can be found in Froidevaux et al. (2006) and Schwartz et al. (2008).  
153        One can see that the NLC field extended mostly from the west to east along an area filled with  
154        low temperatures of 136-146 K, and the NLC were located north of  $58^\circ\text{N}$  due to rapidly  
155        increasing temperature with decreasing latitude. That is why the NLC were observed at low  
156        elevation angles (far to the north as seen from the Moscow region) on this particular night.

157        Detailed analysis of five consecutive in time balloon-borne images (Figs. 4 and 5) has  
158        revealed the following features of the NLC display:

159        a) The horizontal extent of the NLC field from the western to eastern observable border  
160        was about 1450 km, and from the northern to southern border of about 750 km. Such  
161        distances are impossible to observe from the ground due to the Earth's curvature and limited  
162        area of the twilight arch. The central part of the NLC field, having extension of about 850 x  
163        550 km, was seen from the ground but the western and eastern wings of the field as well as  
164        the northern edge were located below the local ground horizon, making it impossible to  
165        observe them. Thus, balloon-borne NLC observations have an obvious great advantage over



166 ground-based observations in terms of larger geographic coverage which is comparable to  
167 PMC observations made from space.

168 b) The southmost edge of the NLC field was modulated by partial circles (something like  
169 ice voids but with open southern border), which is shown by the red curves in Figures 4 and 5.  
170 The diameters of these partial ice voids are estimated to be in the range of 150-250 km. The  
171 mechanism of the formation of ice voids in NLC/PMC is not clear now, and it is an ongoing  
172 topic in atmospheric physics. One can mention three main mechanisms which are currently  
173 discussing in the literature. Trubnikov and Skuratova (1967) addressed a theory of cellular  
174 convection and demonstrated its principal possibility in the summer mesosphere in relation to  
175 NLC occurrences. The authors estimated convective cells to be in the range of 90-250 km in  
176 radius, that agrees well with sizes of partial ice voids obtained in the present study. However,  
177 there should be fulfill the main criterion for the convection to be developed, namely, the  
178 height gradient of the potential temperature should have negative values. We have carefully  
179 estimated the potential temperature gradient or the static stability (based on Aura/MLS  
180 temperature measurements) in the analyzed area and could not find any signatures of its  
181 negative values in the mesosphere and mesopause region. It means that in this particular case  
182 cellular convection could not be responsible for the observed partial ice voids in the NLC.

183 However, satellite measurements can easily miss a negative static stability at local scales  
184 due to poor horizontal resolution and local ice voids may be generated by a gravity wave  
185 breaking. Rusch et al. (2009) have hypothesized that ice voids could be caused by heating due  
186 to the passage of warm crests of a gravity wave. It is possible in the present case. However,  
187 we could not find any significant displacement of the partial ice voids (their boundaries)  
188 relative to the NLC field, i.e., the partial ice voids traveled with the same speed and direction  
189 as the entire NLC field did (~43 m/s from the south to north). One would expect an intrinsic  
190 phase speed and intrinsic direction of the movement of the partial ice voids if they were  
191 generated by a large-scale gravity wave of a wavelength of several hundreds of km. Thus, it is  
192 difficult to prove this hypothesis of the influence of a large-scale gravity wave on the  
193 formation of the observed partial ice voids.

194 Thuraijah et al. (2013b) have proposed another mechanism related to a shock wave  
195 generated by a meteorite, which expands and cools the air that in turn leads to the formation  
196 of large ice particles which fall out of an NLC field (analogously to hole-punch clouds due to  
197 the passage of an aircraft). However, we observe large-scale partial ice voids (150-250 km) in  
198 a broad area of the mesopause over 1000 km. It was hardly possible that any big meteorite



199 could produce such large holes in such broad area, and we did not observe any meteor motion  
200 in our ground-based and balloon images.

201 Megner et al. (2018) have recently presented an interesting case study of a quasi-  
202 stationary ice void in NLC which did not follow the general wind, suggesting that it was  
203 formed by a localized warming at the summer mesopause. This is not the case in our case  
204 study, in which we have observed partial ice voids moving at the general wind speed in the  
205 same direction along with the entire NLC field.

206 In the present case study, the partial ice voids had irregular shape and sizes ranging from  
207 150 to 250 km. Also, these partial voids moved along the wind, having the same speed and  
208 direction. Thus, it is difficult to connect these partial voids with regular wave disturbances. At  
209 the same time, as shown in Fig. 3, the southmost border of the NLC field was confined to the  
210 warm air mass located at sub-polar latitudes of  $\sim 58^\circ\text{N}$  and lower. The mesopause temperature  
211 at this border was equal to  $\sim 147\text{ K}$  at 86 km altitude. The MLS data cannot reproduce the  
212 exact shape of this border due to low horizontal resolution ( $\sim 15^\circ$ ) and temporal resolution of  
213  $\sim 1.5\text{ h}$ . However, it is well known that tropospheric frontal systems have a meandering shape,  
214 sometimes with intrusions of warm and cold air masses as in case of the formation of a frontal  
215 wave cyclone (Ahrens, 1993; Stull, 2000). In our case the warm front at the mesopause and  
216 the NLC partial ice voids resemble a tropospheric frontal wave, in which there are intrusions  
217 of warm air masses, moving from midlatitudes, into the cold air mass located at sub-polar and  
218 polar latitudes (see Fig. 6). Therefore, we consider that the most probable source of these  
219 partial ice voids observed in the NLC in this particular case is the intrusion of warm air  
220 masses into the cold air mass with the NLC field, sublimating ice particles. A similar  
221 conclusion was proposed by Thurairajah et al. (2013a) who have analyzed a large ice void  
222 observed in PMC (using AIM/CIPS satellite images) and have concluded that *“warmer*  
223 *temperatures (warmer than the frost point temperature of  $\sim 144\text{ K}$ ) at the location of the void*  
224 *may be related to increased tidal activity and transport of warm air from low latitudes.*” Also,  
225 Bailey et al. (2009) and Thurairajah et al. (2013b) have demonstrated that southmost borders  
226 of PMC can be highly modulated by partial ice voids of several hundreds of km in diameter,  
227 and the authors have found the structural similarity between PMC images and those seen in  
228 tropospheric clouds.

229 c) Clear vertical modulation of the NLC layer is shown with the red arrow in Fig. 7. This  
230 is a unique view on a particular gravity wave seen at the local horizon of the balloon; that is  
231 why this wave modulation is viewed almost at the right angle to the line-of-sight. This  
232 geometry allows observing a thin layer of NLC modulated in altitude by propagating gravity





233 waves of small and medium scales. Such geometry is almost impossible to obtain from the  
234 ground since NLC seen at the very horizon are usually masked by topography, tropospheric  
235 clouds and, most importantly, by tropospheric aerosols, which are constantly present and  
236 significantly absorb NLC brightness when looking at the very horizon. We have carefully  
237 estimated parameters of this particular wave: its horizontal wavelength was equal to  $49.4 \pm 2.2$   
238 km and its vertical amplitude was  $1.9 \pm 0.1$  km between the crest and trough. In this  
239 calculation, the angle of  $13.3^\circ$  between the camera image plane and vertical plane at the NLC  
240 altitude was taken into account. Also note that since NLC are clearly seen both in the crest  
241 and trough of the wave (ice particles did not completely sublimated in the wave trough), we  
242 have estimated the wave amplitude both in the wave crest and trough. The amplitude  
243 estimations are the same in the wave trough and crest (within the given uncertainty). All this  
244 makes us confident in the estimation of the vertical amplitude of this particular wave. This is  
245 the most precise estimation of the amplitude of a gravity wave at the mesopause by using  
246 NLC observations (Witt, 1962; Haurwitz and Fogle, 1969; Bronshten and Grishin, 1970;  
247 Demissie et al., 2014). Since wave amplitude represents kinetic wave energy, this is an  
248 important source of information for estimating the wave energy budget at the upper  
249 atmosphere, and also can be used for future model studies to estimate a wave source in the  
250 lower atmosphere (Fritts and Alexander, 2003; Demissie et al., 2014).

251 d) Small-scale billow-type gravity waves were estimated to have horizontal wavelengths  
252 of 8-11 km (Fig. 7). Such small-scale gravity waves are well-known to be observed in NLC  
253 layers (Witt, 1962; Dalin et al., 2010; Pautet et al., 2011; Baumgarten and Fritts, 2014;  
254 Demissie et al., 2014), but we demonstrate this result in order to emphasize the ability to  
255 resolve small-scale NLC structures by using a large FoV camera, having a high resolution  
256 sensor, onboard a sounding balloon.

257 e) Figure 8 illustrates an NLC image taken from altitude of 20.3 km which is very close to  
258 the maximum reached altitude of 20.4 km. The NLC were rather faint by that time that is in  
259 line with an idea of the intrusion of warm air masses from mid- to subpolar latitudes. These  
260 large-scale warm air masses led to rapid sublimation of ice particles at large scales of about  
261 1500 km. At the same time, one can see a very interesting feature to be considered. There were  
262 several thin parallel gravity wave bands (stripes) with lengths of 50-200 km and widths of ~  
263 3-5 km in cross-section. The reasons of seeing such thin stripes are as follows: (a) The SONC  
264 balloon was in the stratosphere, i.e., above the troposphere in which optically strong air  
265 turbulence is constantly present (b) The exposure time of this image was very short of 1/125 s.  
266 All these made the image free from blurring (as minimum blurring as possible for moving





267 NLC and balloon motion). This image demonstrates a final stage of the NLC evolution (NLC  
268 disappeared in 20 min since the image was taken), and these thin stripes might represent a  
269 final morphological state of the NLC evolution. Further balloon-borne NLC observations of  
270 very faint NLC are required to confirm this consideration.

271

## 272 **5 Conclusions**

273 The combination of high resolution images (~30 m) and large geographic coverage (over  
274 1500 km) is a unique property intrinsic to stratospheric balloon-borne NLC observations,  
275 which is impossible to achieve either from the ground or space. In general, a balloon-borne  
276 NLC observation provides us with the following new opportunities in case of a long duration  
277 flight of several days:

- 278 a) NLC imagery can be obtained for 24 hours a day and during several days due to very  
279 little Rayleigh atmospheric scattering in the visible subrange of the spectrum above 20 km  
280 (Hughes, 1964);
- 281 b) Quantitative information on a wide range of waves (gravity and planetary waves, solar  
282 tides), propagating through the summer mesopause can be obtained;
- 283 c) Neutral wind velocity at the mesopause and large-scale trajectory of NLC fields over 1500  
284 km can be measured;
- 285 d) Quantitative information on long mesospheric fronts, solitons and other non-linear  
286 processes can be obtained;
- 287 e) Quantitative information on small-scale turbulent structures (down to 1 m) can be  
288 obtained in case of using a narrow field of view lens.
- 289 f) High resolution vertical NLC structure (wave modulation, double layers) can be retrieved  
290 by observing NLC at the very horizon. Absence of any terrain obstacles and tropospheric  
291 aerosol loading makes such stratospheric NLC observations unique.
- 292 g) Absence of optically strong tropospheric turbulence makes NLC images free from  
293 atmospheric blurring that in turn results in well-defined fine structures of gravity waves  
294 and turbulence in the mesopause region.

295

296 In the present study, we have estimated the following characteristics of the NLC field:

- 297 a) The horizontal extent of the NLC field as seen from the SONC balloon was about  
298 1450 x 750 km whereas it was about 800 x 550 km as seen from the ground. This  
299 emphasizes the great advantage of making large-scale balloon-borne observations over



- 300 medium-scale ground-based ones.
- 301 b) NLC field was traveling from the south to north at a mean velocity of 43 m/s;
- 302 c) The southmost edge of the NLC field was modulated by partial ice voids of 150-250  
303 km in diameter, which were like generated by the intrusion of warm air masses  
304 moving from mid- to sub-polar latitudes. The mesopause temperature at this edge was  
305 equal to  $\sim 147$  K, i.e., it was a threshold temperature separating the mesopause region  
306 filled with NLC from the warm area without NLC.
- 307 d) A medium-scale wave had a wavelength of  $49.4 \pm 2.2$  km and vertical amplitude of  
308  $1.9 \pm 0.1$  km. This is the most precise estimation of a gravity wave amplitude ever  
309 made.
- 310 e) Small-scale billow-type gravity waves had wavelengths of 8-11 km.
- 311 f) The final morphology state of the NLC evolution was represented by thin parallel  
312 gravity wave stripes with lengths of 50-200 km and widths of  $\sim 3$ -5 km.

313

314 *Data availability.* The reader can access the SONC experiment images and balloon GPS  
315 coordinates, used in the paper, via publically available project ftp server at the Swedish  
316 Institute of Space Physics: [ftp://ftp.irf.se/outgoing/pdalin/NLC/SONC\\_experiment/](ftp://ftp.irf.se/outgoing/pdalin/NLC/SONC_experiment/)

317

318 *Author contributions.* PD wrote the paper, made calculations and plotted the figures. NP and  
319 VP read and made suggestions appropriated for the paper. DE provided the raw balloon-borne  
320 images and balloon GPS coordinates. VR contributed to the image processing. All the authors  
321 read and commented regarding the work and agreed with the content and submission of this  
322 paper.

323

324 *Competing interests.* The authors declare that they have no conflict of interest.

325

326 *Acknowledgments.* The authors are grateful to Nikolay Gusev, Andrey Reshetnikov, Alexander  
327 Dalin for their support of ground-based NLC observations during the SONC experiment. The  
328 Aura/MLS data version 2.2 were obtained from the NASA Goddard Space Flight Center Data  
329 and Information Services Center: <https://mirador.gsfc.nasa.gov>.

330



331 *Financial support.* The work was partly supported by the Russian Foundation for Basic  
332 Research under project 15-05-04975a.

333

### 334 **References**

- 335 Ahrens, C. D.: Essentials of meteorology: an invitation to the atmosphere, West Publishing  
336 Company, St. Paul, 1993.
- 337 Bailey, S. M., Thomas, G. E., Rusch, D. W., Merkel, A. W., Jeppesen, C., Carstens, et al.:  
338 Phase functions of polar mesospheric cloud ice as observed by the CIPS instrument on the  
339 AIM satellite, *J. Atmos. Sol.-Terr. Phys.*, 71, 3736380,  
340 <http://dx.doi.org/10.1016/j.jastp.2008.09.039>, 2009.
- 341 Baumgarten, G., Fiedler, J., Fricke, K. H., Gerding, M., Hervig, M., Hoffmann, P., et al.: The  
342 noctilucent cloud (NLC) display during the ECOMA/MASS sounding rocket flights on 3  
343 August 2007: morphology on global to local scales, *Ann. Geophys.*, 27, 9536965, 2009.
- 344 Baumgarten, G., and Fritts, D. C.: Quantifying Kelvin-Helmholtz instability dynamics  
345 observed in noctilucent clouds: 1. Methods and observations, *J. Geophys. Res. Atmos.*,  
346 119, 932469337. doi:10.1002/2014JD021832, 2014.
- 347 Bronshten, V. A., and Grishin, N. I.: Noctilucent clouds, Nauka, Moscow, 1970.
- 348 Chandran, A., Rusch, D. W., Palo, S. E., Thomas, G. E., and Taylor, M. J.: Gravity wave  
349 observations in the summertime polar mesosphere from the Cloud Imaging and Particle  
350 Size (CIPS) experiment on the AIM spacecraft, *J. Atmos. Sol.-Terr. Phys.*, 71, 3926400,  
351 doi:10.1016/j.jastp.2008.09.041, 2009.
- 352 Dalin, P., Kirkwood, S., Moström, A., Stebel, K., Hoffmann, P., and Singer, W.: A case study  
353 of gravity waves in noctilucent clouds, *Ann. Geophys.*, 22, 1875-1884, 2004.
- 354 Dalin, P., Pertsev, N., Zadorozhny, A., Connors, M., Schofield, I., Shelton, I., et al.: Ground-  
355 based observations of noctilucent clouds with a northern hemisphere network of  
356 automated digital cameras, *J. Atmos. Sol.-Terr. Phys.*, 70, 146061472, 2008.
- 357 Dalin, P., Pertsev, N., Frandsen, S., Hansen, O., Andersen, H., Dubietis, A., and Balciunas, R.:  
358 A case study of the evolution of a Kelvin-Helmholtz wave and turbulence in noctilucent  
359 clouds, *J. Atmos. Sol.-Terr. Phys.*, 72,14-15, 1129-1138. doi:10.1016/j.jastp.2010.06.011,  
360 2010.
- 361 Dalin, P., Connors, M., Schofield, I., Dubietis, A., Pertsev, N., Perminov, V., et al.: First  
362 common volume ground-based and space measurements of the mesospheric front in  
363 noctilucent clouds, *Geophys. Res. Lett.*, 40, 639966404. doi:10.1002/2013GL058553,  
364 2013.



- 365 Dalin, P., Pogoreltsev, A., Pertsev, N., Perminov, V., Shevchuk, N., Dubietis, A., et al.:
- 366 Evidence of the formation of noctilucent clouds due to propagation of an isolated gravity
- 367 wave caused by a tropospheric occluded front, *Geophys. Res. Lett.*, 42, 2037-2046.
- 368 doi:10.1002/2014GL062776, 2015.
- 369 Dalin, P., Pertsev, N., Perminov, V., Efremov, D., and Romejko, V.: Looking at õnight-
- 370 shiningõ clouds from the stratosphere, *Eos*, 100, <https://doi.org/10.1029/2019EO118439>,
- 371 2019.
- 372 DeLand, M. T., and Thomas, G. E.: Updated PMC trends derived from SBUV data, *J.*
- 373 *Geophys. Res. Atmos.*, 120, 2140-2166, doi:10.1002/2014JD022253, 2015.
- 374 Demissie, T. D., Espy, P. J., Kleinknecht, N. H., Halten, M., Kaifler, N., and Baumgarten, G.:
- 375 Characteristics and sources of gravity waves observed in noctilucent cloud over Norway,
- 376 *Atmos. Chem. Phys.*, 14, 12133612142, doi:10.5194/acp-14-12133-2014, 2014.
- 377 Dubietis, A., Dalin, P., Balciunas, R., Cernis, K., Pertsev, N., Sukhodoev, V., et al.:
- 378 Noctilucent clouds: modern ground-based photographic observations by a digital camera
- 379 network, *Applied Optics*, 50, 28, F72-F79, doi:10.1364/AO.50.000F72, 2011.
- 380 Fiedler, J., Baumgarten, G., Berger, U., Hoffmann, P., Kaifler, N., and Lübken, F.-J.: NLC and
- 381 the background atmosphere above ALOMAR, *Atmos. Chem. Phys.*, 11, 570165717,
- 382 doi:10.5194/acp-11-5701-2011, 2011.
- 383 Fritts, D. C., Isler, J. R., Thomas, G. E., and Andreassen, Ø.: Wave breaking signatures in
- 384 noctilucent clouds, *Geophys. Res. Lett.*, 20, 203962042, doi:10.1029/93GL01982, 1993.
- 385 Fritts, D. C., and Alexander, M. J.: Gravity wave dynamics and effects in the middle
- 386 atmosphere, *Reviews of Geophysics*, 41, 1003, doi:10.1029/2001RG000106, 2003.
- 387 Fritts, D. C., Miller, A.D., Kjellstrand, C.B., Geach, C., Williams, B.P., et al.: PMC Turbo:
- 388 Studying gravity wave and instability dynamics in the summer mesosphere using polar
- 389 mesospheric cloud imaging and profiling from a stratospheric balloon, *J. Geophys. Res.*
- 390 *Atmos.*, 124, <https://doi.org/10.1029/2019JD030298>, 2019.
- 391 Froidevaux, L., Livesey, N. J., Read, W. G., Jiang, Y. B., Jiménez, C. C., Filipiak, M. J., et al.:
- 392 Early validation analyses of atmospheric profiles from EOS MLS on the Aura satellite,
- 393 *IEEE Transactions on Geoscience and Remote Sensing*, 44, 5, 110661121, 2006.
- 394 Gadsden, M., and Schröder, W.: *Noctilucent Clouds*, Springer, New York, 1989.
- 395 Gumbel, J., and Witt, G.: Rocket-borne photometry of NLC particle populations, *Adv. Space*
- 396 *Res.*, 28, 7, 1053-1058, 2001.
- 397 Haurwitz, B., and Fogle, B.: Wave forms in noctilucent clouds, *Deep-Sea Research*, 16, 85-
- 398 95, 1969.



- 399 Hemenway, C. L., Soberman, R. K., and Witt, G.: Sampling of noctilucent cloud particles,  
400 *Tellus*, XVI, 1, 84-88, 1964.
- 401 Hultgren, K., Körnich, H., Gumbel, J., Gerding, M., Hoffmann, P., Lossow, S., and Megner,  
402 L.: What caused the exceptional mid-latitude Noctilucent Cloud event in July 2009, *J.*  
403 *Atmos. Sol.-Terr. Phys.*, 73, 2125-2131, 2011.
- 404 Hughes, J. V.: Sky brightness as a function of altitude, *Applied Optics*, 3, 10, 1135-1138,  
405 1964.
- 406 Karlsson, B., and Gumbel, J.: Challenges in the limb retrieval of noctilucent cloud properties  
407 from Odin/OSIRIS, *Adv. Space Res.*, 36, 935-942, doi:10.1016/j.asr.2005.04.074, 2005.
- 408 Kirkwood, S., and Stebel, K.: Influence of planetary waves on noctilucent clouds occurrence  
409 over NW Europe, *J. Geophys. Res.*, 108, D8, 8440, doi:10.1029/2002JD002356, 2003.
- 410 Liu, X., Yue, J., Xu, J., Yuan, W., Russell III, J.M., Hervig, M. E., and Nakamura, T.:  
411 Persistent longitudinal variations in 8 years of CIPS/AIM polar mesospheric clouds, *J.*  
412 *Geophys. Res. Atmos.*, 121, 839068409, doi:10.1002/2015JD024624, 2016.
- 413 Megner, L., Stegman, J., Pautet, P.-D., and Taylor, M. J.: First observed temporal  
414 development of a noctilucent cloud ice void, *Geophys. Res. Lett.*, 45,  
415 <https://doi.org/10.1029/2018GL078501>, 2018.
- 416 Miller, A. D., Fritts, D. C., Chapman, D., Jones, G., Limon, M., Araujo, D., et al.:  
417 Stratospheric imaging of polar mesospheric clouds: a new window on small-scale  
418 atmospheric dynamics, *Geophys. Res. Lett.*, 42, 605866065, doi:10.1002/2015GL064758,  
419 2015.
- 420 Pautet, P.-D., Stegman, J., Wrasse, C. M., Nielsen, K., Takahashi, H., Taylor, M. J., et al.:  
421 Analysis of gravity waves structures visible in noctilucent cloud images, *J. Atmos. Sol.-*  
422 *Terr. Phys.*, 73, 14-15, 2082-2090, doi: 10.1016/j.jastp.2010.06.001, 2011.
- 423 Pertsev, N., Dalin, P., and Perminov, V.: Influence of semidiurnal and semimonthly lunar  
424 tides on the mesopause as observed in hydroxyl layer and noctilucent clouds  
425 characteristics, *Geomagn. Aeron.*, 55, 6, 8116820, doi:10.1134/S0016793215060109,  
426 2015.
- 427 Rapp, M., Lübken, F.-J., Müllemann, A., Thomas, G., and Jensen, E.: Small scale temperature  
428 variations in the vicinity of NLC: experimental and model results, *J. Geophys. Res.*, 107,  
429 D19, 4392, doi:10.1029/2001JD001241, 2002.
- 430 Reichborn-Kjennerud, B., Aboobaker, A. M., Ade, P., Aubin, F., Baccigalupi, C., Bao, C., et  
431 al.: EBEX: A balloon-borne CMB polarization experiment, *Proceedings of SPIE*,  
432 *Millimeter, Submillimeter and Far-Infrared Detectors and Instrumentation for Astronomy*



- 433 V, San Diego, Calif., USA, 29 June–July 2010, Soc. of Photo-Opt. Instrum. Eng. (SPIE)  
434 Conf. Ser., 7741, edited by W. S. Holland and J. Zmuidzinas, SPIE, Bellingham, Wash.  
435 doi:10.1117/12.857138, 2010.
- 436 Reimuller, J. D., Thayer, J. P., Baumgarten, G., Chandran, A., Hulley, B., Rusch, D., Nielsen,  
437 K., and Lumpe, J.: Synchronized imagery of noctilucent clouds at the day-night terminator  
438 using airborne and spaceborne platforms, *J. Atmos. Sol.-Terr. Phys.*, 73, 14-15, 2091-  
439 2096, 2011.
- 440 Romejko, V. A., Dalin, P. A., and Pertsev, N. N.: Forty years of noctilucent cloud observations  
441 near Moscow: database and simple statistics, *J. Geophys. Res. Atmos.*, 108, D8, 8443,  
442 doi:10.1029/2002JD002364, 2003.
- 443 Schwartz, M. J., Lambert, A., Manney, G. L., Read, W. G., Livesey, N. J., Froidevaux, L., et  
444 al.: Validation of the Aura Microwave Limb Sounder temperature and geopotential height  
445 measurements, *J. Geophys. Res.*, 113, D15S11, 2008.
- 446 Stull, R. B.: *Meteorology for scientists and engineers*, Second Edition, Brooks/Cole, Pacific  
447 Grove, 2000.
- 448 Suzuki, H., Sakanoi, K., Nishitani, N., Ogawa, T., Ejiri, M. K., Kubota, M., Kinoshita, T.,  
449 Murayama, Y., and Fujiyoshi, Y.: First imaging and identification of a noctilucent cloud  
450 from multiple sites in Hokkaido (43.2644.4°N), Japan, *Earth, Planets and Space*, 68, 182,  
451 DOI 10.1186/s40623-016-0562-6, 2016.
- 452 Taylor, M. J., Pautet, P.-D., Zhao, Y., Randall, C. E., Lumpe, J., Bailey, S. M., et al.: High-  
453 latitude gravity wave measurements in noctilucent clouds and polar mesospheric clouds.  
454 In: Abdu M., Pancheva, D. (eds), *Aeronomy of the Earth's Atmosphere and Ionosphere*,  
455 IAGA Special Sopron Book Series, Springer, Dordrecht, 2, 93-105, doi:10.1007/978-94-  
456 007-0326-1\_7, 2011.
- 457 Thomas, G. E.: Solar Mesosphere Explorer measurements of polar mesospheric clouds  
458 (noctilucent clouds), *J. Atmos. Terr. Phys.*, 46, 9, 819-824, 1984.
- 459 Thurairajah, B., Bailey, S. M., Siskind, D. E., Randall, C. E., Taylor, M. J., and Russell III, J.  
460 M.: Case study of an ice void structure in polar mesospheric clouds, *J. Atmos. Sol.-Terr.*  
461 *Phys.*, 104, 224-233, <http://dx.doi.org/10.1016/j.jastp.2013.02.001>, 2013a.
- 462 Thurairajah, B., Bailey, S. M., Nielsen, K., Randall, C. E., Lumpe, J., Taylor, M. J., and  
463 Russell III, J. M.: Morphology of polar mesospheric clouds as seen from space, *J. Atmos.*  
464 *Sol.-Terr. Phys.*, 104, 234-243, <http://dx.doi.org/10.1016/j.jastp.2012.09.009>, 2013b.



- 465 Trubnikov, B. N., and Skuratova, I. S.: Cellular convection in the zone of noctilucent clouds,  
466 Proceedings of the International Symposium on Noctilucent Clouds, Tallinn, 1966, 208-  
467 215, Eds. I.A. Khvostikov and G. Witt, VINITI, Moscow, 1967.
- 468 Witt, G.: Height, structure and displacements of noctilucent clouds, *Tellus*, 14, 1, 1618, 1962.
- 469 Zadorozhny, A. M., Tyutin, A. A., Witt, G., Wilhelm, N., Wälchli, U., Cho, J. Y. N., and  
470 Swartz, W. E.: Electric field measurements in the vicinity of noctilucent clouds and PMSE,  
471 *Geophys. Res. Lett.*, 20, 20, 2299-2302, 1993.





472 **Figure captions:**

473 **Figure 1.** The 3-axis motorized gimbal stabilized platform, holding the NLC camera,  
474 designed and build by the Aerospace laboratory ãStratonauticaö. Photo by Denis Efremov.  
475

476 **Figure 2.** (Left) the altitude of the SONC balloon as a function of time flight. (Right) the  
477 vertical-horizontal trajectories of the SONC balloon: the red line is the upleg and the black  
478 line is the downleg trajectories.  
479

480 **Figure 3.** The temperature map at the mesopause (86.1 km) as measured by the Aura/MLS  
481 spectrometer on 5 July 2018. Nighttime measurements around the globe have been selected to  
482 produce the map. Upon the temperature map, the outer borders of the NLC field are  
483 overplotted: the red line is as seen from the SONC balloon, the black line is as seen from the  
484 ground at the launch. The black dots mark the position of the balloon at 7.8 km at the ground  
485 and ground-based observers.  
486

487 **Figure 4.** The NLC field as observed from the SONC balloon at 4092 m, 4947 m, 7836 m,  
488 9077 m and 13928 m above the ground at 21:46 UT, 21:49 UT, 21:57 UT, 22:01 UT, 22:20  
489 UT on 5 July 2018. The red curves indicate large areas free from NLC particles (partial ice  
490 voids).  
491

492 **Figure 5.** Projection of the NLC fields (shown in Figure 4) as observed from the SONC  
493 balloon on the surface. The red curves indicate large areas free from NLC particles (partial ice  
494 voids).  
495

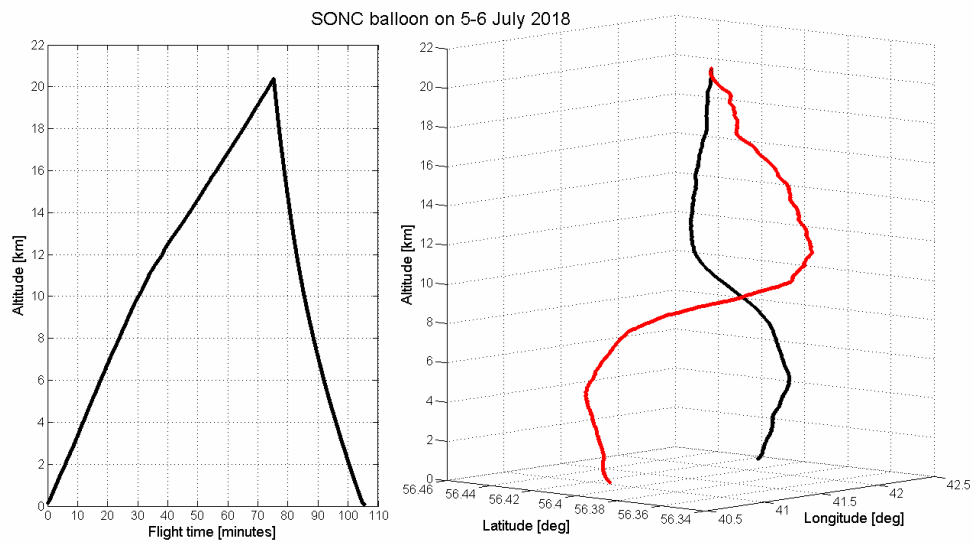
496 **Figure 6.** A schematic representation of the intrusion of warm air masses from mid- to sub-  
497 polar latitudes, forming partial ice voids in the observed NLC. A general concept of this  
498 scheme is analogous to the formation of a wave cyclone in the troposphere (see Figs. 8.18 and  
499 8.19 in Ahrens, 1993).  
500

501 **Figure 7.** The SONC balloon image taken at 6222 m above the ground at 21:49 UT on 5 July  
502 2018. The red arrow marks the vertical modulation of the NLC layer by a gravity wave of  
503 medium scale. The green arrow indicates small-scale billow-type gravity waves.  
504

505 **Figure 8.** The SONC balloon image taken at 20.3 km above the ground at 22:48 UT on 5 July  
506 2018 represents the final stage of NLC evolution on that night.

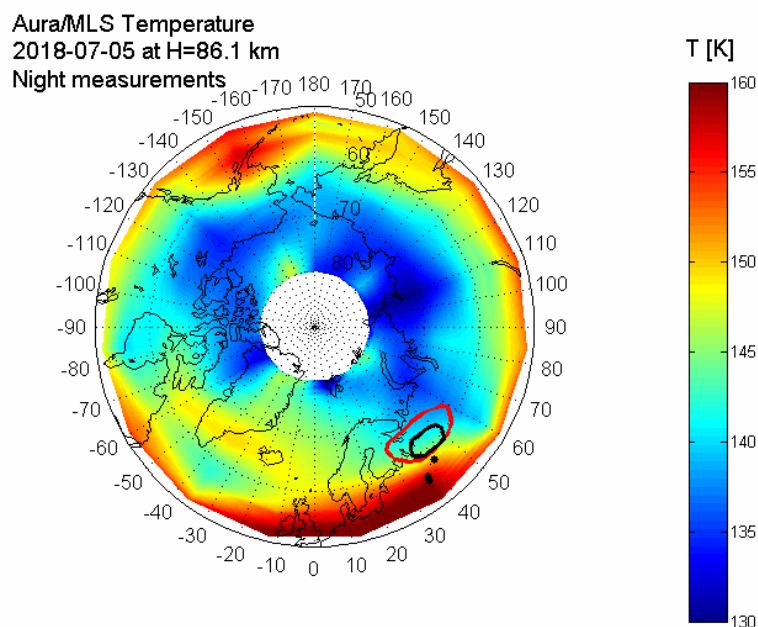


507  
508 **Figure 1.** The 3-axis motorized gimbal stabilized platform, holding the NLC camera,  
509 designed and built by the Aerospace laboratory "Stratonautica". Photo by Denis Efremov.



510

511 **Figure 2.** (Left) the altitude of the SONC balloon as a function of time flight. (Right) the  
512 vertical-horizontal trajectories of the SONC balloon: the red line is the upleg and the black  
513 line is the downleg trajectories.



514

515 **Figure 3.** The temperature map at the mesopause (86.1 km) as measured by the Aura/MLS  
516 spectrometer on 5 July 2018. Nighttime measurements around the globe have been selected to  
517 produce the map. Upon the temperature map, the outer borders of the NLC field are  
518 overplotted: the red line is as seen from the SONC balloon, the black line is as seen from the  
519 ground at the launch. The black dots mark the position of the balloon at 7.8 km at the ground  
520 and ground-based observers.



521

522 **Figure 4.** The NLC field as observed from the SONC balloon at 4092 m, 4947 m, 7836 m,  
523 9077 m and 13928 m above the ground at 21:46 UT, 21:49 UT, 21:57 UT, 22:01 UT, 22:20  
524 UT on 5 July 2018. The red curves indicate large areas free from NLC particles (partial ice  
525 voids).

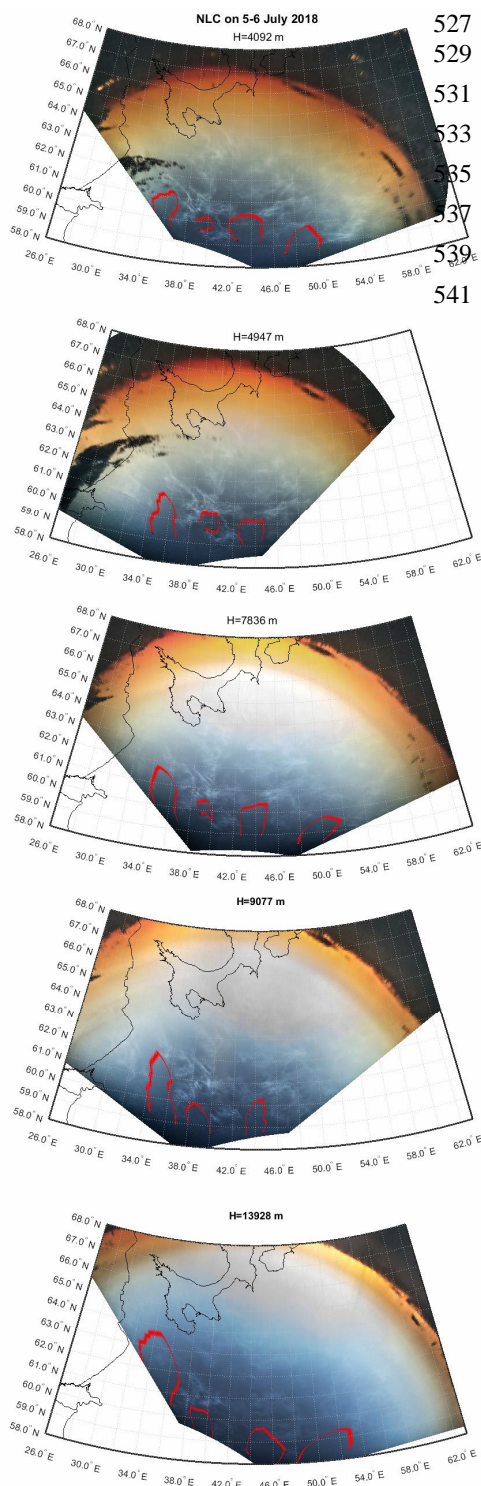
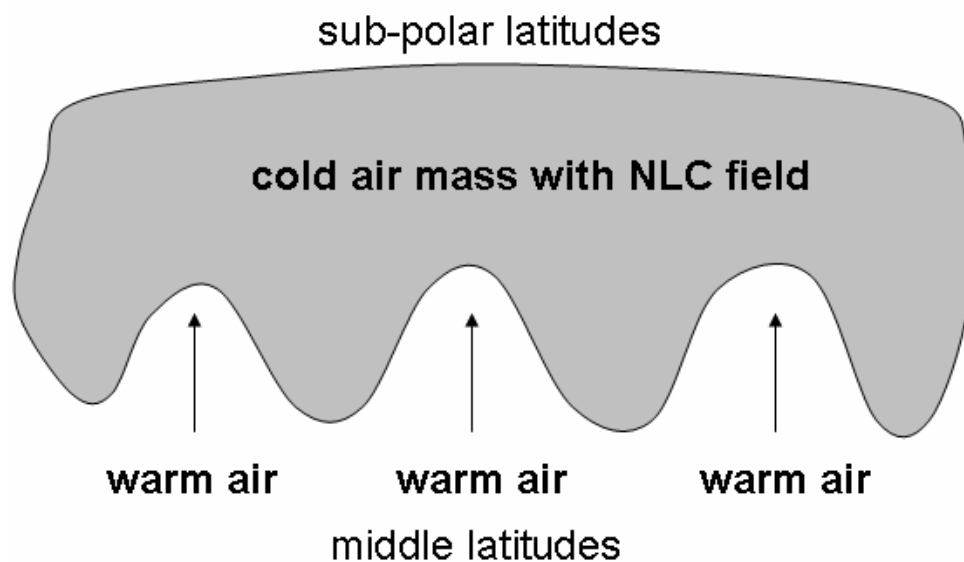


**Figure 5.** Projection of the NLC fields (shown in Figure 4) as observed from the SONC balloon on the surface. The red curves indicate large areas free from NLC particles (partial ice voids).

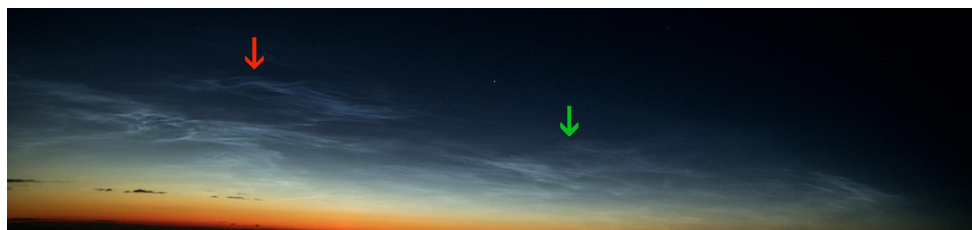
527  
529  
531  
533  
535  
537  
539  
541





542  
543 **Figure 6.** A schematic representation of the intrusion of warm air masses from mid- to sub-  
544 polar latitudes, forming partial ice voids in the observed NLC. A general concept of this  
545 scheme is analogous to the formation of a wave cyclone in the troposphere (see Figs. 8.18 and  
546 8.19 in Ahrens, 1993).





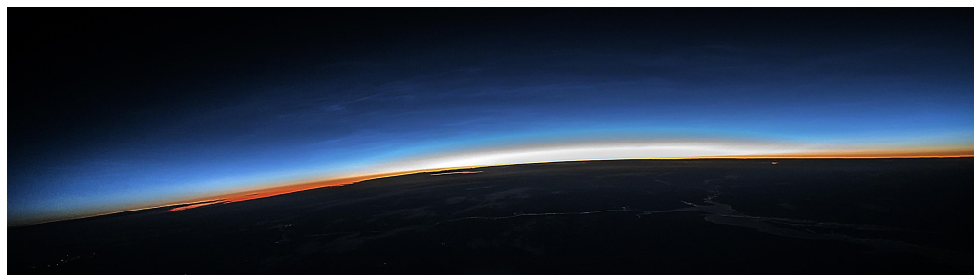
547

548

549 **Figure 7.** The SONC balloon image taken at 6222 m above the ground at 21:49 UT on 5 July

550 2018. The red arrow marks the vertical modulation of the NLC layer by a gravity wave of

551 medium scale. The green arrow indicates small-scale billow-type gravity waves.



552

553

554 **Figure 8.** The SONC balloon image taken at 20.3 km above the ground at 22:48 UT on 5 July

555 2018 represents the final stage of NLC evolution on that night.

556